J Solid State Electrochem (2007) 11: 71–76
DOI 10.1007/s10008-005-0071-1

ORIGINAL PAPER

C. Leger · S. Bach · J-P. Pereira-Ramos

The sol–gel chromium-modified V_6O_{13} as a cathodic material for lithium batteries

Received: 28 June 2005 / Revised: 11 July 2005 / Accepted: 9 September 2005 / Published online: 11 November 2005
© Springer-Verlag 2005

Abstract A new V_6O_{13}-based material has been synthesized via the sol–gel route. This sol–gel mixed oxide has been obtained from an appropriate heat treatment of the chromium-exchanged V_2O_5 xerogel performed under reducing atmosphere. This new compound, with the chemical formula $Cr_{0.36}V_6O_{13.50}$, exhibits a monoclinic structure ($C2/m$) with the following unit cell parameters, a=11.89 Å, b=3.68 Å, c=10.14 Å, β=101.18°. The electrochemical characterization of this compound has been performed using galvanostatic discharge–charge experiments in the potential range 4–1.5 V and completed by ac impedance spectroscopy measurements. It exhibits a specific capacity of about 370 mAh g^{-1}, which makes the compound $Cr_{0.36}V_6O_{13.50}$ the best one in the V_6O_{13}-based system: 85% of the initial capacity (315 mAh g^{-1}) after the 35th cycle is still available at $C/25$ without any polarization. From impedance spectroscopy, a high kinetics of Li transport (D_{Li}=1.8×10^{-9} cm^2 s^{-1}) is found at mid-discharge.

Keywords Vanadium oxide · Sol–gel process · Lithium batteries

Introduction

Many studies have focused on secondary non-aqueous lithium batteries that use vanadium oxides, such as V_2O_5, LiV_3O_8 or $V_6O_{13\pm\delta}$, as a cathode because of their high energy densities and good cycling capabilities [1–3]. Each one of these compounds exhibits advantages and drawbacks. V_6O_{13}, with its open structure combined with a high content of V^{5+} and V^{4+}, is capable of reaching high capacities. However, the electrochemical behaviour is strongly dependent on the stoichiometry of this compound, $V_6O_{13\pm\delta}(-0.2 \leq \delta \leq 0.3)$. Indeed, this cathode material allows a maximum lithium uptake varying from 1.24 to 1.36 Li per vanadium [4, 5]. After several cycles, the maximum average capacity achievable in the case of an optimized non-stoichiometric $V_6O_{13\pm\delta}$ appears to be ≈0.7 F per vanadium [2]. Another drawback is the difficulty of synthesizing a single-phase material $V_6O_{13\pm\delta}$ [6–8]. The resulting compound consists, in fact, of a mixture of close structures, a monoclinic $V_6O_{13\pm\delta}$ and a monoclinic phase VO_2(B).

The sol–gel process can be used for the synthesis of this kind of compounds. Sol–gel process chemistry provides homogeneous mixing of reactants on the molecular level and can also be used to control shape, morphology and particle size in the resulting products. Previous results obtained in our group have shown the benefit of using the sol–gel method to obtain new and/or high-performance cathodic materials, especially in the case of V_2O_5-based compounds and MnO_2 oxides [9, 10]. For instance, we have performed the synthesis of a chromium vanadium oxide $Cr_{0.11}V_2O_{5.16}$ obtained by a thermal treatment at 550 °C in air from a chromium–vanadium xerogel [9]. The presence of chromium and additional oxygen atoms results in an improvement (10%) of the specific capacity available (350 mAh g^{-1}) after 50 cycles in comparison with that achieved with the V_2O_5 parent oxide [9, 11].

In this paper, we report on the sol–gel synthesis combined with an appropriate heat treatment leading to a new binary oxide $Cr_{0.36}V_6O_{13.50}$. The effect of experimental parameters including temperature and time of the thermal treatment is also presented. The electrochemical behaviour of this new compound is examined as a possible positive material for rechargeable batteries.

Experimental

The basic material is V_2O_5 gel, with formula $V_2O_5{\cdot}nH_2O$, prepared by spontaneous polycondensation of decavanadic acid [12]. The latter was obtained by dropping an aqueous solution of sodium metavanadate on an ion-exchange resin (Dowex 50WX2, 50–100 mesh). The red viscous V_2O_5 gel

C. Leger · S. Bach (✉) · J.-P. Pereira-Ramos
Laboratoire d'Electrochimie Catalyse et Synthèse Organique,
C.N.R.S. UMR 7582,
2, rue Henri-Dunant,
94320 Thiais, France
e-mail: bach@glvt-cnrs.fr

obtained readily loses most of its water at room temperature, leading to the xerogel $V_2O_5(OH^-)_{0.33}(H_3O^+)_{0.33}(H_2O)$, named VXG. This compound is composed of flat ribbons about 10^3 Å long, 10^2 Å wide and 10 Å thick. An ion-exchange procedure performed in a $Cr(NO_3)_3{\cdot}6H_2O$ aqueous solution allows to obtain the chromium-exchanged xerogel $V_2O_5(OH^-)_{0.33}(Cr^{3+})_{0.11}(H_2O)$, named Cr-VXG. Intercalation does not modify the order related to the stacking of the ribbons [12].

X-ray diffraction (XRD) experiments were performed with a Philips PW 1830 diffractometer using the CoK_α radiation (λ=1.7889 Å).

Chemical composition of the compound was checked by elemental analysis using inductively coupled plasma-mass spectrometry (ICP-MS) and by atomic emission spectrometry. By these method, the mean oxidation state of vanadium (Z_V) was determined by a chemical method using ferrous ammonium sulphate with an accuracy of ±2%: the powder sample is dissolved in an aqueous solution containing concentrated H_2SO_4. The V(V) ions appearing during the dissolution of the sample are titrated with an aqueous solution of ferrous ammonium sulphate.

The electrochemical characteristics were determined with three-electrode electrochemical cells. The working electrode consisted of a stainless-steel grid on which the cathodic material was pressed. The cathode was made of a mixture of active material (80 wt%) with graphite (7.5 wt%), acetylene black (7.5 wt%) and polytetrafluoroethylene (PTFE, 5 wt%). The mixture is pressed onto a stainless-steel grid, with a geometric area of 1 cm^2. The counter electrode consisted of a lithium foil and the reference electrode of a lithium wire in a separate compartment. The electrolyte used was 1 M $LiClO_4$ in propylene carbonate (PC). PC, double-distilled, was obtained from Fluka and used as received. Anhydrous lithium perchlorate was dried under vacuum at 200 °C for 12 h. Electrochemical measurements were made with a potentiostat PAR 273 A coupled to an IBM 386 computer. Impedance spectroscopy was carried out in the frequency range 10^4–10^{-4} Hz using an EG&G (PAR) potentiostat coupled with a Schlumberger 1255 Frequency Response Analyser. The excitation signal was 10 mV peak to peak. The equilibrium potential was considered to be reached when the drift in open-circuit voltage remained less than 1 m V during 5 h.

Results and discussion

Theobald et al. [6] have reported that the thermal treatment of V_2O_5 in a reducing atmosphere, hydrogenated argon (Ar/10% H_2) led to a mixture of V_6O_{13} and VO_2(B).

When the Cr-VXG is heat-treated at 520 °C in air, a new orthorhombic mixed oxide is obtained [9]. In that case, it has been shown that during heat treatment, Cr^{3+} ions were located in an octahedral environment in the V_2O_5 planes with additional oxygen atoms above and below [9] to form short Cr_2O_3 chains along the *c*-axis. Therefore, we decided to apply such a heat treatment to the Cr-VXG but under reducing atmosphere in order to stabilize a mixed oxide with an oxidation state lower than 5.

The XRD patterns of the products obtained after heating of the starting material Cr-VXG at 400 °C in a reducing atmosphere, hydrogenated argon (Ar/10% H_2) for different time durations are reported in Fig. 1. The changes observed in the XRD patterns of Fig. 1 clearly indicate that the nature of the resulting products strongly depends on the reaction time. After the heat treatment performed at 400 °C for 7 h (Fig. 1a), most of the diffraction peaks still confirm the presence of V_2O_5, labeled A, but also the presence of

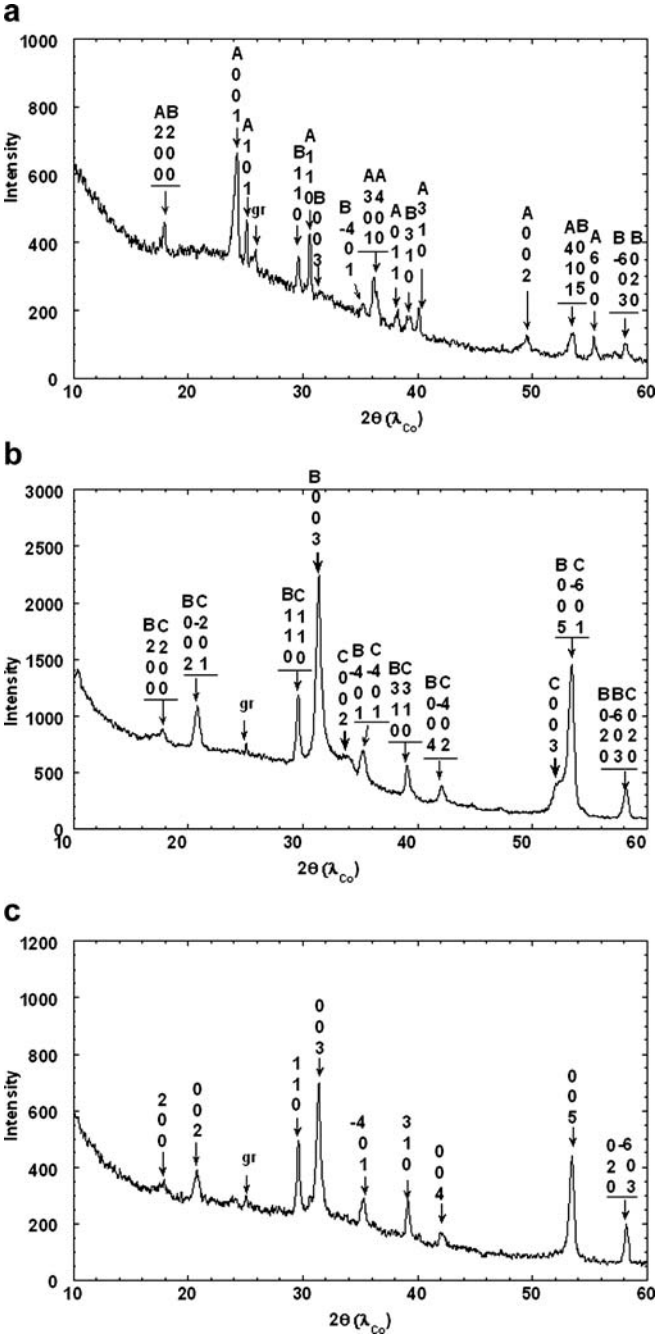

Fig. 1 XRD patterns of Cr-VXG heat-treated for 7 h (**a**), 12 h (**b**) and 7 and 5 h with a second grinding (**c**). *A* V_2O_5, *B* $V_6O_{13+\delta}$, *C* VO_2(B) (*gr* grease)

$V_6O_{13\pm\delta}$, which is revealed by the (110) and (003) small diffraction lines at 2θ values=29.52° and 31.5° (labeled B). To the contrary, when the reaction time is further extended to 12 h, the reduction process is more efficient. Indeed, the typical XRD pattern characteristic of $V_6O_{13\pm\delta}$ (labeled B) coexists with an important amount of an allotropic crystalline structure of vanadium dioxide, VO_2(B), as indicated by the diffraction lines, 200, $\bar{2}01$, 110, $\bar{4}01$, 310, $\bar{4}02$, 003, $\bar{6}01$ and 020 (labeled C) (Fig. 1b). In fact, these diffraction lines can belong to the two different systems, $V_6O_{13\pm\delta}$ and VO_2(B), both being characterized by a monoclinic symmetry. However, the strong line located at 2θ=31.25° (003) belongs only to the $V_6O_{13\pm\delta}$ system, while two other lines located at 2θ=33.76° (002) and at 2θ=51.74° (003) were characteristic of VO_2(B). This result shows the presence of these two phases in samples heat-treated at 400 °C for 12 h. In a third attempt, the Cr-VXG compound is successively treated at 400 °C for about 7 h and then ground for 20 min before a second heat treatment for 5 h. In this case, all the diffraction lines can be indexed on the basis of $V_6O_{13\pm\delta}$ (Fig. 1c). The disappearance of the two diffraction lines (002) and (003) at 2θ=33.76° and 51.74°, respectively, demonstrates unambiguously the presence of a single-phase compound $V_6O_{13\pm\delta}$ with a monoclinic structure ($C2/m$) and the following unit cell parameters: a=11.89 Å, b=3.68 Å, c=10.14 Å, β=101.18°. These values are close to those reported in [4, 5, 7, 14] from a thermal treatment of V_2O_5 in hydrogenated argon (Ar/10% H_2). No additional phase due to a chromium oxide such as Cr_2O_3 is present. All these results are consistent with the probable presence of chromium ions in the structure of V_6O_{13}. The structure of this compound contains distorted VO_6 octahedra joined by edge sharing into single and double zigzag chains linked together by additional edge sharing into single and double sheets of octahedra parallel to the (100) plane (Fig. 2). Using the measured oxidation state of vanadium in the oxide (Z_V=4.32±0.02, i.e. 32% of V^{5+} and 68% of V^{4+}), the initial amount of Cr^{3+} present in the Cr-VXG and the chemical composition determined by elementary analysis (0.06 ±0.01 Cr per V), a convenient formula for the new mixed oxide (Fig. 1c) is $Cr_{0.36}V_6O_{13.50}$, i.e. $Cr_{0.36}{}^{III}V_{1.9}{}^{V}V_{4.10}{}^{IV}O_{13.50}$. It has been found that the similar heat-treatment procedure applied to the VXG led to a mixture of V_2O_5, V_3O_7 and V_6O_{13}. This provides evidence that the chromium ions play a predominant role by acting as an additional reducing agent, allowing the formation of a single phase of V_6O_{13}.

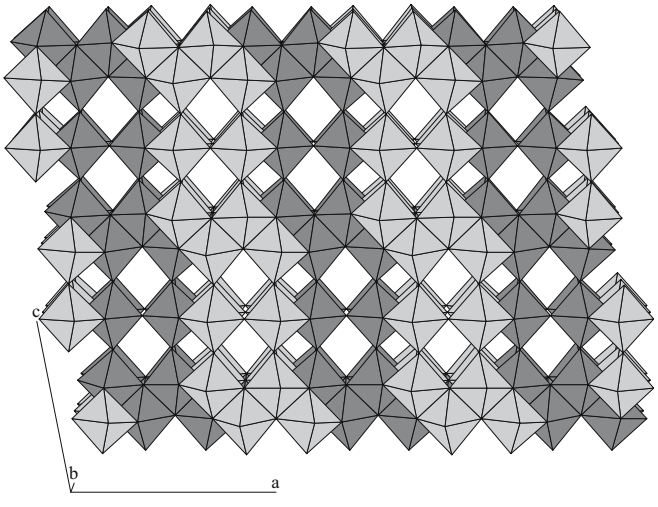

Fig. 2 Monoclinic structure of V_6O_{13} (a=11.89 Å, b=3.68 Å, c=10.14 Å, β=101.18°)

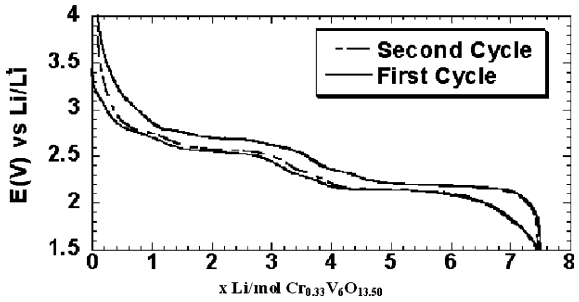

Fig. 3 First and second discharge–charge profile curves for the sol–gel mixed oxide $Cr_{0.36}V_6O_{13.50}$ in 1 M $LiClO_4$ solution in PC at C/25 discharge–charge rate

Fig. 3 shows the discharge–charge profile of $Cr_{0.36}V_6O_{13.50}$ at C/25. Three reduction processes appear in galvanostatic curves. The first step is characterized by an important decrease of the working potential from its initial value of 3.42 up to 2.60 V and involves a faradaic yield of 1.4 F/mol oxide. The second and third steps appear as a voltage plateau located at 2.55 and 2.1 V, respectively, and correspond to the accommodation of 2.5 and 3.5 additional lithium ions in the host lattice of $Cr_{0.36}V_6O_{13.50}$. This profile is similar with other discharge curves reported for $V_6O_{13\pm\delta}$ cathodes ($-0.2\leq\delta\leq0.3$) [2, 4, 5, 7, 8, 15, 16]. This overall faradaic yield of 7.5 F/mol is consistent with the theoretical one according to West et al. [4] and involves the quantitative reduction of all V^{5+} into V^{4+}, then V^{4+} into V^{3+}, but only obtained from OCV experiments. Other works performed on $V_6O_{13\pm\delta}(-0.2\delta0.3)$ ($-0.2\leq\delta\leq0.3$) report faradaic yield which never exceeds 6–7.1$Li^+/V_6O_{13\pm\delta}$ (Table 1) [2, 4, 5, 15, 16]. Moreover, in the case of stoichiometric V_6O_{13}, smaller faradaic yield with values between 3.3 and 4.5 Li^+/V_6O_{13} [2, 4, 5] are obtained. A complete removal of Li^+ ions from the oxide was achieved during the charge process performed up to the cut-off voltage of 4 V. Of particular interest is the close operating voltage (around 100 mV) for the reduction and oxidation processes. This probably indicates a similar kinetics for Li transport in the oxide for insertion and deintercalation as well as a

Table 1 Maximum lithium uptake of various $V_6O_{13\pm\delta}$ as a function of δ and of the number of cycles (values from literature data)

	$V_6O_{13+\delta}$				
	δ=−0.14	δ=0	δ=0.14	δ=0.16	δ=0.28
First reduction of x in $Li_xV_6O_{13\pm\delta}$	6.6 [2]	3.3 [2]; 4.5 [4]; 3.6 [5]	5.4 [4]	6 [5]; 7.1 [15]	5 [16]
After nth cycles x in $Li_xV_6O_{13\pm\delta}$	40 [2] 3.9 [2]	80 [2] 3.2 [2]	25 [4] 4.2 [4]	5 [5] 4.2 [5]	150 2.5 [16]

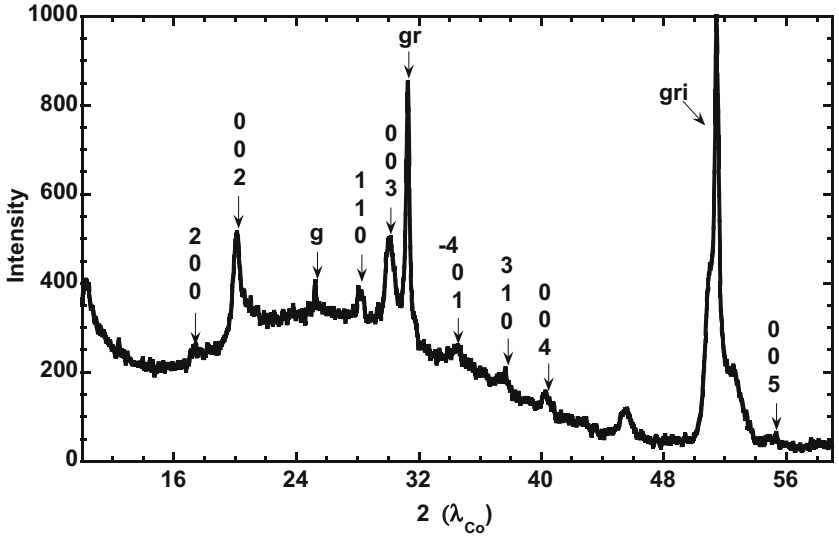

Fig. 4 XRD pattern of $Li_{7.5}Cr_{0.36}V_6O_{13.50}$ obtained at the end of the first discharge (*g* graphite, *gr* grease)

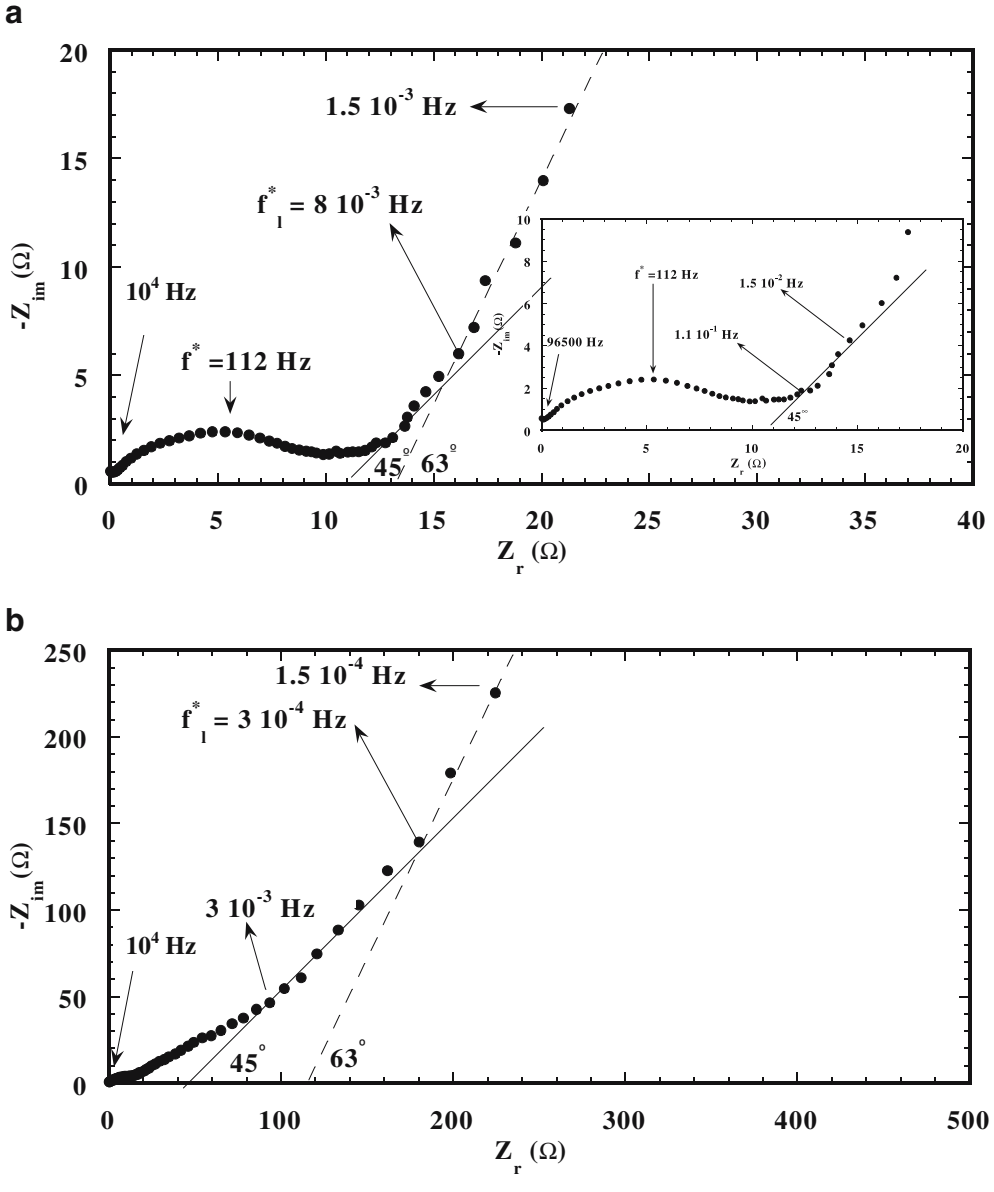

Fig. 5 AC impedance diagrams for various values of *x* in $Li_xCr_{0.36}V_6O_{13.50}$, **a** x=3.8, **b** x=7.5

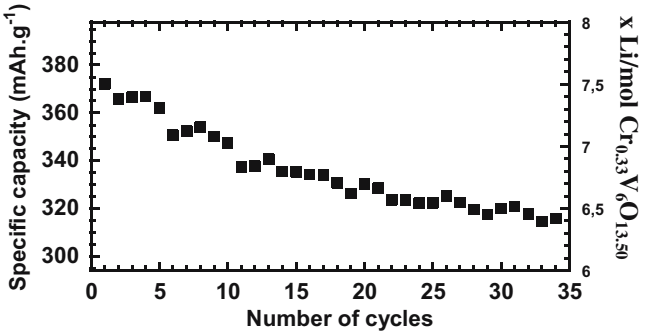

Fig. 6 Evolution of the specific capacity for a $Cr_{0.36}V_6O_{13.50}$-based electrode as a function of the number of cycles [cycling limits 4–1.5 V, *C*/25]

reversible behaviour. The first and second discharge–charge curves are superimposed, showing the high reversibility of the Li insertion–extraction reaction in $Cr_{0.36}V_6O_{13.50}$. From these results, it appears that this new cathodic material is one of the most promising rechargeable vanadium oxide forms for Li batteries with a specific capacity of 370 mAh g^{-1} against only 325 mAh g^{-1} for the best result reported on $V_6O_{13+\delta}$ [2].

The analysis of the XRD diffraction pattern obtained for a composite electrode with the $Li_{7.5}Cr_{0.36}V_6O_{13.50}$ composition, i.e. obtained at the end of the first discharge, indicates the crystal structure of the V_6O_{13} model is preserved with the unit cell parameters (a=12.8 Å, b=3.88 Å, c=10.51 Å and β=100.60°) (Fig. 4). However, the accommodation of around 7.5 Li/mol oxide induces an expansion of all the unit cell parameters a, b and c, corresponding to a significant change by 13% of the volume of the unit monoclinic cell.

Typical ac impedance diagrams obtained for $Li_{3.8}Cr_{0.36}V_6O_{13.50}$ and $Li_{7.5}Cr_{0.36}V_6O_{13.50}$ are reported in Fig. 5. These diagrams present three regions: in the high-frequency range (10^4–10 Hz), a semicircle corresponding to the charge transfer is obtained with a characteristic frequency f^*≈110 Hz, with a charge transfer resistance, R_{tc}, in the range 10–20 Ω. The shape of this high-frequency region changes with the Li content. From a perfect defined semicircle which joins the real axis for $Li_{3.8}Cr_{0.33}V_6O_{13.50}$ (Fig. 5a), it changes to a less well defined shape for $Li_{7.5}Cr_{0.36}V_6O_{13.50}$ (Fig. 5b). For this Li content, a highly distorted diagram in the high- and medium-frequency ranges is obtained, indicating the time constants of the different physical processes are not well separated. This indicates a more porous character of the electrode, which has to be related with the considerable volume expansion of the unit cell of the oxide at high depth of discharge as discussed above for $Li_{7.5}Cr_{0.36}V_6O_{13.50}$. Another information displayed by this first analysis of impedance diagrams consists in the continuous increase of the cathode impedance from 130 Ω for $Li_{3.8}Cr_{0.36}V_6O_{13.50}$ to 220 Ω for $Li_{7.5}Cr_{0.36}V_6O_{13.50}$.

The low-frequency response is characterized by a straight line with a phase angle of 45° from the real axis, corresponding to the Warburg impedance from which the numerical values of D_{Li} are calculated using Eq. 1 when $\omega >> 2D_{Li}/L^2$ [17]:

$$D_{Li} = \left[\frac{V_M}{F \cdot \sqrt{2}} \cdot \left(\frac{dE}{dx}\right)_x \cdot \frac{1}{A \cdot S}\right]^2 \quad (1)$$

where V_M is the molar volume of the compound (=52 cm^3 mol^{-1}), S is the apparent surface area of the electrode, i.e. 1 cm^2, and $(dE/dx)_x$ is the slope, at fixed x, of the equilibrium potential composition curve. L is the maximum length of the diffusion pathway (cm). The analysis of the Warburg impedance of the system plotted in the complex plane $-ImZ = A\omega^{-1/2}$ or $ReZ = A\omega^{-1/2}$ allows to obtain the Warburg prefactor A and then to calculate D_{Li}. This region corresponds to a frequency range where the kinetics of the system is almost entirely limited by the rate of the chemical diffusional process in the host material under semi-infinite conditions. Its position in frequency significantly depends on the lithium content in $Li_xCr_{0.36}V_6O_{13.50}$. For instance, the frequency range of the Warburg region changes from 1.1×10^{-1}–1.5×10^{-2} Hz for x=3.8 (Fig. 5a) to 3×10^{-3}–3×10^{-4} Hz for x=7.5 (Fig. 5b). This qualitatively indicates a decrease of the chemical Li diffusion coefficient D_{Li} when x increases, while the kinetics of the charge transfer does not change. For $Li_{3.8}Cr_{0.36}V_6O_{13.50}$, a high value of D_{Li} is found, around 1.8×10^{-9} cm^2 s^{-1}, while a lower value of D_{Li}, around 7×10^{-11} cm^2 s^{-1}, is obtained for $Li_{7.5}Cr_{0.36}V_6O_{13.50}$. Finally, at lower frequencies (10^{-3}–10^{-4} Hz), the 45° line begins to give way to a vertical line (i.e. the phase angle is increasing) corresponding to the finite diffusion process. Calculation of the length for the diffusion pathway (L) can be then performed from the limiting frequency, f_l, using Eq. (2): $\omega_L = (2D_{Li}/L^2)$. For the determination of L, we used the value of D_{Li} calculated from the Warburg impedance using Eq. 1 when $\omega >> 2D_{Li}/L^2$ [17]. It can be noticed that we obtained a good determination of D_{Li} because we found value of L around 1.9 μm for $Li_{3.8}Cr_{0.36}V_6O_{13.50}$, consistent with the grain size ($\varnothing_{particles}$=2.5 μm) evaluated from laser granulometry and MEB experiments ($\varnothing_{particles} \neq 2L$). These results are consistent with kinetic data on Li transport in V_6O_{13} [4] with values around 10^{-10}–10^{-11} cm^2 s^{-1} decreasing with high lithium contents, and other works on Li diffusion in other vanadium oxides, such as

Table 2 Vanadium and chromium contents in the electrolyte after 40 cycles at T=25 °C at C/25 rate

Compound	At the end of the 40th reduction (C/25)
$Cr_{0.36}V_6O_{13.50}$	$\%V = \frac{\text{Number of moles of V present in the electrolyte}}{\text{Number of moles of V in the initial electrode}} \times 100 = 0.56 \pm 0.04$
	$\%Cr = \frac{\text{Number of moles of Cr present in the electrolyte}}{\text{Number of moles of Cr in the initial electrode}} \times 100 = 3.1 \pm 0.2$

V_2O_5, give data which vary from 10^{-9} up to 10^{-12} cm^2 s^{-1} [18–20].

The evolution of the specific capacity for $Cr_{0.36}V_6O_{13.50}$ is depicted as a function of cycles number at *C*/25 rate in the potential window 4–1.5 V (Fig. 6). The trend in the cycling behaviour of $Cr_{0.36}V_6O_{13.50}$ is a decrease of the specific capacity from 370 to 320 mAh g^{-1} during the first 20 cycles to reach 315 mAh g^{-1} after 35 cycles, which corresponds to a faradaic yield of 6.5 F/mol. The appearance of a blue-green color in electrolyte suggests a possible dissolution could occur during cycling. Indeed, Table 2 summarizes data on the vanadium and chromium contents in electrolyte analysed after 40 cycles by ICP-OES compared with the vanadium and chromium contents in the pristine material. It comes out that the amount of vanadium (0.56% of the initial amount of vanadium) and chromium (3.1% of the initial amount of chromium) found in electrolyte can be correlated with the capacity decay observed at *C*/25 rate but does not quantitatively account for the magnitude of the capacity loss. Another possible explanation for the capacity decline could be found in the important change in the volume of the material by 13%, inducing an important loss of contact between particles, leading then to a less efficient electrochemical process even if high values of D_{Li} have been obtained.

However, in spite of this initial capacity decline, the capacity available after 35 cycles is around 320 mAh g^{-1}. This result is the best one reported in the literature [2, 4, 5, 13, 14] for $V_6O_{13+\delta}$ cathodes, as can be seen in Table 1. West et al. [4] report a specific capacity of 210 mAh g^{-1} (4.2 Li^+/V_6O_{13}) after 25 cycles. Other cycling galvanostatic tests performed on oxygen-deficient or surstoichiometric compounds $V_6O_{12.86}$ [4], $V_6O_{13.14}$ [2], $V_6O_{13.16}$ [5] or $V_6O_{13.28}$ [16] report capacities between 210 and 120 mAh g^{-1} mol^{-1} oxide, respectively. Only Barker et al. [21] report similar specific capacities (335 mAh g^{-1}) after hundred cycles, on a parent oxide reported as V_6O_{14}. Hence, the sol–gel mixed oxide $Cr_{0.36}V_6O_{13.50}$ can be considered with interest as 3 V Li intercalation compound. A pillaring effect in the compound due to the incorporation of chromium ions in the structure may be explained by the enhanced capacity.

Acknowledgement The authors are appreciative of assistance from P. Soudan in the chemical characterization of the materials.

References

1. Desilvestro J, Haas O (1990) J Electrochem Soc 137:5C
2. Abraham KM, Goldman JL, Holleck GL (1981) J Electrochem Soc 128:271
3. Delmas C, Cognac-Auradou H, Cocciantelli JM, Menetrier M, Doumerc JP (1994) Solid State Ionics 69:257
4. West K, Zachau-Christiansen B, Jacobsen T (1983) Electrochim Acta 28:1829
5. Murphy DW, Christian PA, DiSalvo FJ, Carides JN, Waszczak JV (1981) J Electrochem Soc 128:2053
6. Theobald F, Cabala R, Bernard J (1976) J Solid State Chem 17:431
7. Lampe-Önnerud C, Nordblad P, Thomas JO (1995) Solid State Ionics 81:189
8. Lampe-Önnerud C, Gustafsson T, Thomas JO (1993) MRS Proc 293:49
9. Soudan P, Pereira-Ramos JP, Farcy J, Gregoire G, Baffier N (2000) Solid State Ionics 135:291
10. Bach S, Henry M, Livage J (1990) J Solid State Chem 88:325
11. Leger C, Bach S, Soudan P, Pereira-Ramos JP (2005) Solid State Ionics 176:1365
12. Aldebert P, Baffier N, Gharbi N, Livage J (1981) Mater Res Bull 16:669
13. Bouhaous A, Aldebert P, Baffier N, Livage J (1985) Rev Chim Miner 22:17
14. Wilhelmi KA, Waltersson K, Khilborg L (1971) Acta Chem Scand 25:2675
15. Saidi MY, Barker J (1995) Solid State Ionics 78:169
16. Menetrier M, Levasseur A, Delmas C (1989) Mater Sci Eng B3:103
17. Ho C, Raistrick ID, Huggins RA (1980) J Electrochem Soc 127:343
18. Zachau-Christiansen B, West K, Jacobsen J (1983) Solid State Ionics 9–10:399
19. Tretyakov YD, Popov AV, Metlin YD (1985) Solid State Ionics 17:265
20. Pistoia G, Temperoni C, Cignini P, Icovi M, Panero S (1980) J Electroanal Chem 108:169
21. Barker J, Saidi ES, Saidi MY (1995) Electrochim Acta 40:94